Targeting ^{V600E}B-Raf and Akt3 Using Nanoliposomal-Small Interfering RNA Inhibits Cutaneous Melanocytic Lesion Development

Melissa A. Tran,[1] Raghavendra Gowda,[1] Arati Sharma,[1,6,7] Eun-Joo Park,[4] James Adair,[5,6] Mark Kester,[1,6] Nadine Barrie Smith,[4,6] and Gavin P. Robertson[1,2,3,6,7]

Departments of [1]Pharmacology, [2]Pathology, [3]Dermatology, [4]Bioengineering, and [5]Material Science and Engineering; [6]Melanoma Therapeutics Program; and [7]Foreman Foundation for Melanoma Research, The Pennsylvania State University, Hershey, Pennsylvania

Abstract

Most events promoting early melanoma development are yet to be identified, but deregulation of the B-Raf and Akt3 signaling cascades is an important regulator of this process. Approximately 90% of normal moles and ~60% of early invasive cutaneous melanomas contain a T1799A *B-Raf* mutation (^{V600E}B-Raf), leading to 10 times higher enzyme activity and constitutive activation of the mitogen-activated protein kinase pathway. Furthermore, ~70% of melanomas have elevated Akt3 signaling due to increased gene copy number and PTEN loss. Therefore, targeting ^{V600E}B-Raf and Akt3 signaling is necessary to prevent or treat cutaneous melanocytic lesions. Agents specifically targeting these proteins are needed, having fewer side effects than those inhibiting both normal and mutant B-Raf protein or targeting all three Akt isoforms. In this study, a unique nanoliposomal-ultrasound–mediated approach has been developed for delivering small interfering RNA (siRNA) specifically targeting ^{V600E}B-Raf and Akt3 into melanocytic tumors present in skin to retard melanoma development. Novel cationic nanoliposomes stably encapsulate siRNA targeting ^{V600E}B-Raf or Akt3, providing protection from degradation and facilitating entry into melanoma cells to decrease expression of these proteins. Low-frequency ultrasound using a lightweight four-cymbal transducer array enables penetration of nanoliposomal-siRNA complex throughout the epidermal and dermal layers of laboratory-generated or animal skin. Nanoliposomal-mediated siRNA targeting of ^{V600E}B-Raf and Akt3 led to a cooperatively acting ~65% decrease in early or invasive cutaneous melanoma compared with inhibition of each singly with negligible associated systemic toxicity. Thus, cationic nanoliposomes loaded with siRNA targeting ^{V600E}B-Raf and Akt3 provide an effective approach for targeted inhibition of early or invasive cutaneous melanomas. [Cancer Res 2008;68(18):7638–49]

Introduction

Melanoma is a cancer of pigmented skin cells called melanocytes residing at the epidermal-dermal junction (1). Most genetic alterations promoting development of early melanomas are yet to be identified. One frequent change occurring in ~90% of normal moles is a T1799A mutation of *B-Raf* in the mitogen-activated protein (MAP) kinase pathway (2–5). Approximately 60% of advanced-stage metastatic melanomas also contain the activating V600E mutation leading to 10.7 times higher activity than occurs in normal cells, thereby promoting cellular proliferation (2–5).

A second frequent alteration promoting melanoma development is increased Akt3 activity in ~70% of melanomas (6). Akt3 is activated through loss of the PTEN phosphatase and increased gene copy number, leading to deregulation of apoptosis, thereby promoting chemoresistance (6, 7). Targeting ^{V600E}B-Raf or Akt3 signaling decreases melanoma tumor development, and simultaneous inhibition can lead to cooperatively acting tumor inhibition (6, 8, 9). Thus, agents specifically targeting ^{V600E}B-Raf and/or Akt3 could have significant potential to treat moles, early melanocytic lesions, or skin metastases in which these proteins are deregulated.

Inhibition of B-Raf or Akt3 using small interfering RNA (siRNA) specifically designed to inhibit ^{V600E}B-Raf but not wild-type B-Raf or Akt3 but not Akt1 or Akt2 protein expression can effectively decrease melanoma tumor development in mice (6, 8, 10). Because these agents target specific genes, there would be fewer potential side effects than with drugs inhibiting both mutant and wild-type B-Raf or all three Akt isoforms (6, 8, 10). Introduction of siRNA in cultured cells is easily accomplished using standard transfection methods (11–13). However, its use as a targeted chemopreventive or therapeutic agent is limited due to degradation in animal systems (14, 15).

Encapsulating siRNA into nanoliposomes can be used for protection and systemic delivery, leading to tumor inhibition (16–18). In contrast, topical administration on skin leads to uptake confined to the upper epidermal layers without complete skin penetration (19). This is due, in part, to skin architecture, with epidermis and dermis protected by a surface keratinized layer (19, 20), which prevents most topically applied agents from reaching early melanocytic lesions developing at the epidermal-dermal junction or from reaching locally invasive cutaneous melanoma metastases in the skin dermis (21). One promising strategy for delivery through the keratinized layer is the use of low-frequency ultrasound to permeabilize the skin, enabling passage of macromolecules, including antisense oligonucleotides without significant skin damage (21–26). Combining the protective qualities of nanoliposomes with the permeabilizing activities of low-frequency ultrasound is a novel unexplored strategy for delivering siRNA into melanocytic lesions present in skin to prevent or treat cutaneous melanoma.

This study details the development of a unique nanoliposomal-ultrasound–mediated approach for delivering siRNA targeting

Requests for reprints: Gavin P. Robertson, Department of Pharmacology, R130, The Pennsylvania State University College of Medicine, 500 University Drive, Hershey, PA 17033. Phone: 717-531-8098; Fax: 717-531-5013; E-mail: gprobertson@psu.edu.

doi:10.1158/0008-5472.CAN-07-6614

^{V600E}B-Raf and Akt3 protein expression into melanocytic lesions present in skin to inhibit early lesion development or prevent cutaneous melanoma metastasis.

Materials and Methods

Cell lines and culture conditions. Human melanoma cell lines, UACC 903, UACC 903-GFP, 1205 Lu, and C8161.Cl9, and human fibroblasts, FF2441, were maintained in DMEM (Invitrogen) supplemented with 10% fetal bovine serum (FBS; Hyclone). WM35 and WM35-GFP cells were grown as described previously (27). Human keratinocytes, HFK, were grown in Epilife Medium with Human Keratinocyte Growth Supplement (Cascade Biologics). Mouse melanocytes, melan-a, were grown in RPMI 1640 (Mediatech) supplemented with 10% FBS, 2 mmol/L L-glutamine, and 200 nmol/L 12-*O*-tetradecanoylphorbol-13-acetate (Sigma-Aldrich).

Liposome composition, characterization, and siRNA loading. Nanoliposomes were created by combining 1,2-dioleoyl-3-trimethylammonium-propane (DOTAP), 1,2-dioleoyl-*sn*-glycero-3-phosphoethanolamine (DOPE), and 1,2-distearoyl-*sn*-glycero-3-phosphoethanolamine-*N*-[amino(polyethylene glycol)2000] [DSPE-PEG(2000); Avanti Polar Lipids] in chloroform at a 4.75:4.75:0.5 molar ratio (28, 29). siRNA and nanoliposomes complexing occurred at specific weight ratios of 1:5, 1:10, and 1:15 for 0.5 to 24 h. A quasielastic light scattering system (Malvern Nanosizer, Malvern Instruments) was used to measure the particle diameter of nanoliposomes ± siRNA 1 d after preparation. Nanoliposomal loading of siRNA was measured by mixing fluorescent, Alexa Fluor 546–tagged siRNA (Qiagen) with nanoliposomes at specific weight ratios (1:5, 1:10, 1:15) and complexing at room temperature for 0.5, 3, or 6 h. Loading was considered complete when no free siRNA was evident with complex remaining in well of a 2% agarose gel. To measure liposome-mediated protection of siRNA, nanoliposomes complexed with siRNA overnight were treated with 50% FBS for 10, 30, 60, 180, or 360 min. Following FBS treatment, half of the complex at each time point was treated with 0.5% SDS for 10 min at 37°C to disrupt the complexes and release free siRNA. siRNA alone was also digested with 50% FBS at each time point to serve as a control. All samples were run on a 2% agarose gel at 100 V for 20 min and visualized under UV.

Nanoliposomal toxicity. To assess cytotoxicity of nanoliposomes complexed with siRNA in normal or cancer cells, 5×10^3 fibroblasts (FF2441), keratinocytes (HFK), melanocytes (melan-a), and melanoma (1205 Lu) cells were plated into 96-well plates and, 48 h later, treated with ghost nanoliposomes for 24 h at nanoliposomal concentrations of 12.5, 25, and 50 μmol/L or exposed to 125, 250, 500, 1,000, or 2,000 nmol/L of siRNA complexed with nanoliposomes and compared with untreated control cells. Cytotoxicity was analyzed using the CellTiter 96 aqueous nonradioactive cell proliferation assay (Promega).

Uptake of nanoliposomal-siRNA into cells. Uptake and internalization of nanoliposomal-siRNA into cells was determined using Alexa Fluor 546– and/or fluorescein-tagged siRNA (Invitrogen). 1205 Lu cells (1×10^5) were plated and, following overnight growth, nanoliposomal-siRNA complex (100 nmol/L) or ghost nanoliposomes were added. Three hours later, cells were trypsinized and plated onto coverslips followed by overnight incubation. Uptake of siRNA-nanoliposomal complex by fibroblasts (FF2441), keratinocytes (HFK), or melanocytes (melan-a) was measured by plating 5×10^3 cells onto coverslips and, 2 d later, adding nanoliposomal-siRNA (50, 100, or 200 nmol/L) for 3 h. Following all conditions, cells were rinsed with PBS, fixed in 4% parafomaldehyde (Fisher Scientific) for 30 min, washed in PBS, mounted in 4′,6-diamidino-2-phenylindole–containing mountant (Vector Laboratories), and analyzed by fluorescence microscopy to measure uptake.

Nucleofection of siRNA into cells. Stealth siRNA (1.5–200 pmol; Invitrogen) was introduced via an Amaxa Nucleofector into 1×10^6 UACC 903, UACC 903-GFP, or C8161.Cl9 cells using Solution R/Program K-17 or into WM35-GFP cells using NHEM-NEO Solution/Program U-20. Resulting transfection efficiency was ~99% (8). Duration of siRNA-mediated protein knockdown at 0, 2, 4, 6, and 8 d following nucleofection was measured for B-Raf or C-Raf by Western blot analysis. Cells used in reconstructed skin were nucleofected with buffer, siMutB-Raf (100, 50, or 12.5 pmol), siC-Raf (100 pmol), or scrambled (100 pmol) siRNA; plated onto culture dishes; and, 2 d later, mixed with keratinocytes, which was added onto the dermis as detailed below. Protein lysates of remaining cells were analyzed by Western blotting.

Western blot analysis. Western blot analysis was conducted as described previously (30). Blots were probed with primary antibodies to pErk, pMek (Cell Signaling Technologies), B-Raf, extracellular signal–regulated kinase (Erk)-2, Cyclin D1, and C-Raf and secondary antibodies conjugated with horseradish peroxidase (Santa Cruz Biotechnology). Immunoblots were developed with the enhanced chemiluminescence detection system (Amersham Pharmacia Biotech). Blots were normalized to Erk2 and quantified using ImageJ software (31).

Nanoliposomal-siRNA–mediated protein knockdown. 1205 Lu cells (5×10^5) were plated onto six-well plates for 2 d and nanoliposomal-siMutB-Raf or nanoliposomal-siScrambled complex (1 μmol/L) was added. Protein lysates were collected 18 and 32 h later for Western blot analysis to measure B-Raf and Erk2 expression. Protein levels were quantified from three independent blots using ImageJ software, normalized to Erk2, and average B-Raf levels were calculated (31).

Generation of skin containing melanocytic lesions. To create skin in a culture dish, human fibroblasts were trypsinized and resuspended in 10% reconstitution buffer, 10% 10× DMEM (Mediatech), 2.4 μL/mL of 10 mol/L NaOH, and 80% collagen I (Becton Dickinson) at a concentration of 2.5×10^5/mL on ice (32). Mixture was then aliquoted into 6- or 12-well plates and incubated at 37°C for 3 h. E-medium was added to each well to equilibrate the dermal matrix (32). After 2 d of growth, keratinocytes and melanoma cells (WM35-GFP or UACC 903-GFP) were trypsinized and resuspended at a 1:10 ratio of melanoma cells (nucleofected or untreated) to keratinocytes in E-medium. One milliliter of cell suspension was added to each well on top of the dermal layer. Following 2 d of growth, reconstructed skin was transferred onto wire grids and fed via diffusion from E-medium below the platforms.

Ultrasound transducer design and calibration. The cymbal transducer is a novel thin flextensional transducer capable of producing very low frequencies (33, 34). It has a compact, lightweight structure with an adjustable resonance frequency. Caps on the lead zirconate-titanate ceramic contain a shallow cavity beneath the inner surface. The fundamental mode of vibration is flexing of the end caps caused by radial motion of the ceramic. Therefore, the overall displacement of the device is a combination of the axial motion of disk plus radial motion amplified by the end caps (23, 24). A radiofrequency signal was generated by a frequency pulse/function generator (Agilent 32250A) and amplified using an amplifier (model 40A12, Amplifier Research). Electrical impedance of the array was tuned to the output impedance of the amplifier by an external inductor-capacitor tuning network. Pulse period, duty cycle, and exposure time of radiofrequency signal from the frequency generator were monitored using an oscilloscope (Tektronix 2213A). For experiments, signal generator operated at 20 kHz with pulse duration of 200 ms and pulse repetition period of 1 s (i.e., 20% duty cycle); the amplifier gain was set to 50 dB. Pulsed ultrasound was used to avoid heat generation, which could damage array or skin.

Ultrasound treatment and analysis of damage, nanoliposomal-siRNA uptake, and tumor inhibition in reconstructed skin. Skin reconstructs were treated with ultrasound at a frequency of 20 kHz and duty cycle of 20% for 20 min by removing media and submersion in PBS (26). The nanoliposomal-siRNA complex (1 μmol/L) was then applied topically and allowed to soak into the skin. Skin damage was assessed following ultrasound treatment, addition of ghost liposome, and fixation in 4% paraformaldehyde at 4°C overnight. H&E-stained paraffin-embedded cross sections were examined for skin damage by microscopy. Skin reconstruct uptake studies involved treating with nanoliposomes containing 1 μmol/L Alexa Fluor 546–tagged siRNA or ghost nanoliposomes and uptake was analyzed using stereo fluorescence microscopy 1 h later. Skin reconstructs were treated with ultrasound followed by treatment with nanoliposomes containing B-Raf siRNA or ghost nanoliposomes on alternate days from days 10 to 21. Skin reconstructs from all experiments were fixed in 4% paraformaldehyde at 4°C overnight. After fixation, skin was stored in 0.5 mol/L EDTA (pH 8.0; Fisher Scientific). The total average area occupied

by green fluorescent protein (GFP)–tagged tumor nodules present in four to six skin images per skin was used to quantify differences between treatment groups using the IP Lab software.

Cell doubling time. *In vitro* doubling time of UACC 903 cells nucleofected with siRNA was estimated by plating 3×10^3 UACC 903 cells in 96-well plates and at 24-h intervals, using the SRB assay (Sigma) to measure growth rate and calculate doubling times (8).

***In vivo* cell proliferation.** For mechanistic studies, 5×10^6 UACC 903 cells nucleofected with siRNA were injected into mice, and tumors were harvested 4 d later to quantify cell proliferation in formalin-fixed tumor sections using the RPN 20 cell proliferation kit (Amersham Pharmacia Biotech; ref. 8).

Anchorage-independent growth. UACC 903 cells (1×10^6) were nucleofected with siAkt3 (200 pmol), siMutB-Raf (3, 6, or 12 pmol), siScrambled, or buffer; allowed to recover for 2 d; and then plated in serum-free DMEM (2×10^4 per well) onto polyHEMA-coated 96-well plates. Cell viability was assessed 3 d later using the 3-(4,5-dimethyl-thiazol-2yl)-5-(3-carboxymethoxyphenyl)-2-(4-sulfophenyl)-2*H*-tetrazolium (MTS) assay (9).

Ultrasound and siRNA-nanoliposomal complex treatment of tumors. UACC 903-GFP cells (1×10^6) were injected s.c. into the right flank of nude mice. After 24 h, mice were ultrasound treated for 15 min followed by topical application of 25-μg nanoliposomal-siRNA (siMutB-Raf, siAKt3, or siScrambled) complex on alternate days. For combination nanoliposomal ^{V600E}B-Raf and Akt3 siRNA studies, mice were treated with the same regimen as the single agents. Single agents were compensated with extra liposomes so that equivalent amounts were used. Before ultrasound treatment, mice were anesthetized using 2:1 ketamine/xylazine, and area was sterilized with alcohol pads. Aquaflex Gel Pads (Parker Laboratories, Inc.) served as an ultrasound standoff. Ultrasound was administered for 15 min at a frequency of 20 kHz and duty cycle of 20% (26). Nanoliposomal-siRNA was applied to ultrasound-treated area overlying the tumor for penetration into skin.

Toxicity analysis in mice. To establish toxicity associated with ultrasound plus siRNA-nanoliposomal complex, nude mice were ultrasound treated for 15 min followed by topical addition of nanoliposomal-siRNA (siMutB-Raf, siAkt3, siScrambled, or siMutB-Raf + siAkt3) complex on alternate days. Mice were weighed on alternate days to ascertain toxicity. Following euthanization on day 23, blood was collected from mice and serum separated to measure aspartate aminotransferase (AST), alanine aminotransferase (ALT), glucose, and alkaline phosphatase. Livers were fixed in formalin, sectioned, and stained with H&E to assess liver morphology changes.

Statistical analysis. One-way or two-way ANOVA followed by appropriate post hoc test (Tukey's or Bonferroni) or *t* test was used to ascertain whether significant differences occurred between groups. Differences were considered significant at $P < 0.05$. Combination index was calculated using the Chou-Talalay method with CalcuSyn software to establish mechanistic basis for cooperative inhibition mediated by siRNA targeting ^{V600E}B-Raf and Akt3 (35).

Results

Development of stable cationic nanoliposomes that load siRNA. Because nanoliposomes have been reported as potential siRNA delivery vehicles, a number of possible formulations were evaluated and a novel DOTAP/DOPE/DSPE-PEG(2000) ratio of 4.75:4.75:0.5 was found to efficiently load siRNA. Loading was measured by adding Alexa Fluor 546–tagged siRNA to nanoliposomes at ratios of 1:5, 1:10, or 1:15 (siRNA/liposome, by weight) and complexed for 0.5, 3, or 6 hours. Measuring free fluorescently tagged siRNA present in the gel or as a siRNA-liposome complex retained in the gel well was used to directly assess siRNA loading. A 1:5 ratio following a 0.5-hour incubation showed the presence of both loaded and unloaded siRNA, which was in contrast to the 1:10 and 1:15 ratios where siRNA remained in gel wells, indicating complete complexing with nanoliposomes (Fig. 1*A, top left*). Because maximal loading occurred following 30-min incubation at a 1:10 ratio, this siRNA-nanoliposomal complex formulation was used for subsequent experiments. The diameter of siRNA-liposome complexes 1 day after preparation was measured by dynamic light scattering, showing an average diameter of ~50 nm with a range of 34 to 67 nm (Fig. 1*A, top right*). Ghost nanoliposomes had a similar diameter averaging ~48 nm with a range of 32 to 64 nm. Thus, stable nanoliposomes were generated that loaded siRNA.

siRNA in nanoliposomes is protected from serum degradation. To evaluate the protective effects conferred by nanoliposomes on siRNA, fluorescently tagged free siRNA or siRNA-liposome complexes were exposed to 50% FBS, which is rich in RNA degrading factors, for 10, 30, 60, 180, or 360 minutes. Partial degradation of free siRNA was observed after 10 minutes and complete degradation was observed at 60 minutes (Fig. 1*A, bottom left*). In contrast, siRNA-nanoliposomal complexes remained in gel wells at all time points, indicating protection from degradation (Fig. 1*A, bottom middle*). Half of the original sample was treated with 0.5% SDS for 10 minutes, disrupting the complex and releasing siRNA, which was then run on an agarose gel. Similar levels of free siRNA were observed at all time points, indicating protection by the complex (Fig. 1*A, bottom right*). Thus, siRNA in nanoliposomes was protected from degradation by external factors.

Nanoliposomal-siRNA complex is nontoxic and taken up into the cytoplasm of normal as well as cancer cells. To determine nanoliposomes mediated cellular uptake of siRNA, fibroblasts, keratinocytes, and melanocytes were treated with ghost nanoliposomes or nanoliposomes containing Alexa Flour 546–tagged siRNA (50, 100, or 200 nmol/L). Fluorescence microscopy showed red Alexa fluorescence in ~100% of all cells, indicating uptake of nanoliposomal-siRNA (Fig. 1*B*). To verify that siRNA was taken into the cytoplasm of cells, 1205 Lu cells were treated with 100 nmol/L fluorescein-tagged siRNA-nanoliposomal complex or ghost nanoliposomes. Cells were then trypsinized to remove cell surface–bound nanoliposomes and replated overnight followed by fixation (36). Fluorescence microscopy showed the presence of green fluorescein–tagged siRNA in cytoplasm of cells surrounding a nuclear shadow, indicating that nanoliposomal-siRNA was internalized (Fig. 1*C*). In contrast, no green fluorescence was observed in cells treated with ghost nanoliposomes. Next, toxicity mediated by ghost nanoliposomes was examined in fibroblast, keratinocyte, melanocyte, or 1205 Lu melanoma cells. Cells were treated with increasing concentrations of ghost nanoliposomes (12.5, 25, and 50 μmol/L) for 24 hours and analyzed by MTS assay (37). Compared with untreated cells, no significant decrease in cellular viability was observed, indicating that ghost nanoliposomes were not toxic at the concentrations examined (Fig. 1*D*). The toxicity of siRNA-nanoliposomal complex was next examined in 1205 Lu cells, comparing untreated cells to those treated with increasing concentrations of complex loaded with scrambled siRNA (Fig. 1*D*). No change in cell viability was observed, indicating negligible toxicity. Thus, the siRNA-liposome complex was nontoxic and taken up into the cytoplasm of normal and cancer cells.

siRNA targeting ^{V600E}B-Raf specifically decreases mutant, but not wild-type, protein expression in cells. siRNA can be designed overlapping the T1799A mutation site of ^{V600E}B-Raf, which has potential to selectively decrease the expression of mutant, but not wild-type, protein (8, 10, 30). To verify the specificity of siRNA targeting ^{V600E}B-Raf, 100 pmol (1 μmol/L) was nucleofected into melanoma cells containing mutant (UACC 903) or wild-type protein (C8161.Cl9). Western blot and densitometric

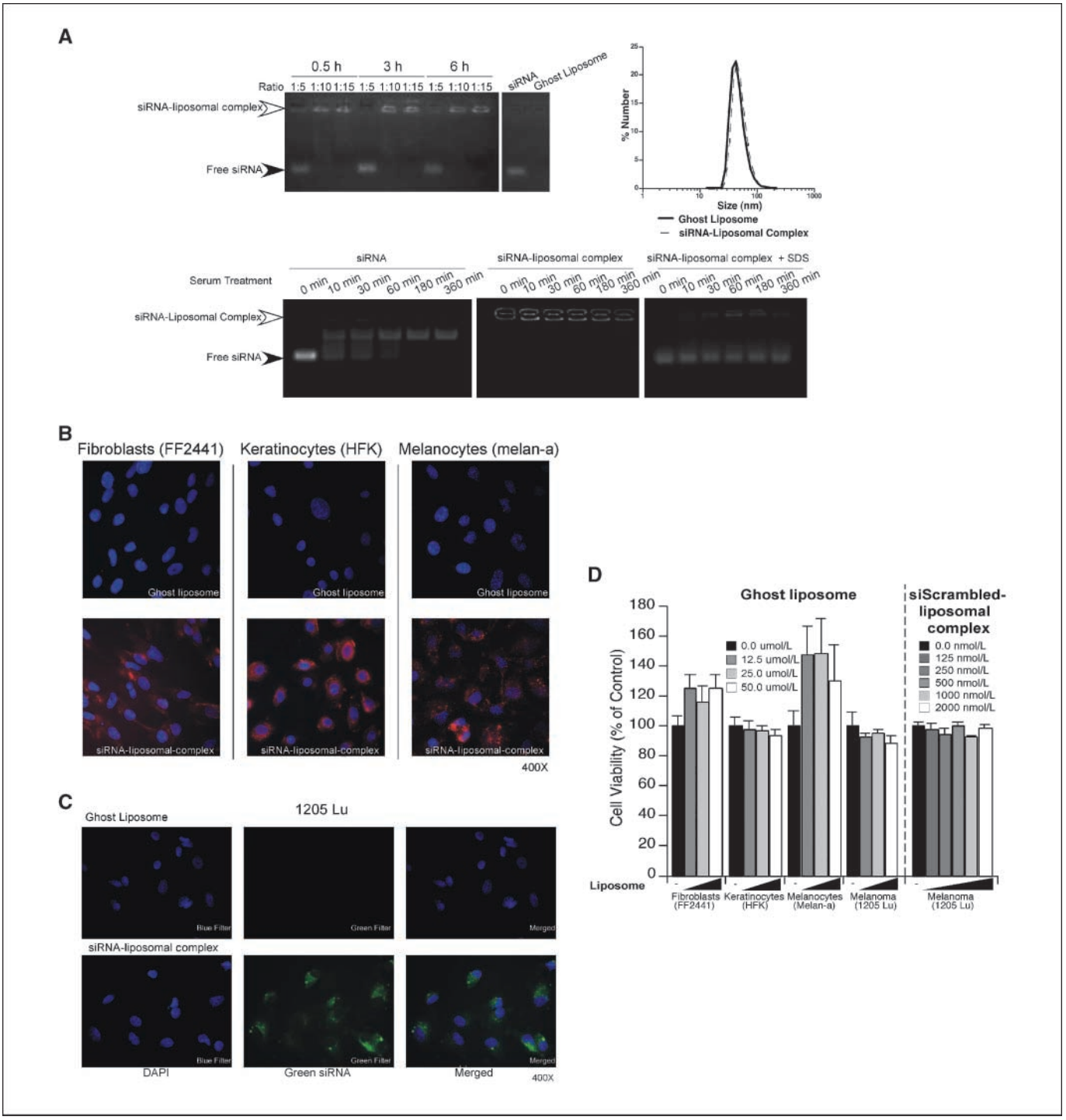

Figure 1. Characterization of cationic siRNA-liposome complexes. *A,* loading of fluorescently tagged siRNA into nanoliposomes. Fluorescently tagged siRNA was complexed with cationic nanoliposomes at ratios of 1:5, 1:10, or 1:15 for 0.5, 3, or 6 h and run on a 2% agarose gel to determine loading efficiency. Maximal loading was reached at a 1:10 ratio following a 0.5-h incubation (*top left*). siRNAs at a 1:10 ratio with nanoliposomes were sized using dynamic light scattering and similar size ranges were observed for ghost or nanoliposomes loaded with siRNA (*top right*). siRNA protection by cationic nanoliposomes was measured by complexing fluorescent siRNA with nanoliposomes overnight followed by exposure to serum for 10, 30, 60, 180, or 360 min. Free fluorescent siRNA alone was used as a control (*bottom left* and *middle*). Release of siRNA in nanoliposomes was accomplished by collapsing serum-treated siRNA-nanoliposomal complexes with SDS to release free siRNA, which was then run on an agarose gel (*bottom right*). *B,* siRNA-nanoliposomal complex is taken up into normal cells. Uptake of siRNA-nanoliposomal complex into normal cells was measured by adding fluorescently tagged siRNA-nanoliposomal complex (200 nmol/L) to fibroblasts, keratinocytes, and melanocytes for 3 h followed by fixation and imaging by fluorescence microscopy (magnification, ×400). Ghost nanoliposomes lacking fluorescent siRNA were used as a control. *C,* siRNA-nanoliposomal complex is taken up into the cytoplasm of cells and is not merely surface bound. siRNA-nanoliposomal complex localization in cells following treatment with siRNA-nanoliposomal complexes (100 nmol/L) was ascertained by exposing 1205 Lu melanoma cells for 3 h, after which cells were trypsinized to remove surface-bound complex and replated overnight onto coverslips. Cells were fixed and imaged by fluorescence microscopy (magnification, ×400). *D,* ghost liposome or siRNA-nanoliposomal complex exerted negligible toxicity on normal or cancer cells. Cellular toxicity of ghost liposome and siRNA-nanoliposomal complex was measured by adding nanoliposomes (12.5, 25, and 50 μmol/L) to fibroblasts, keratinocytes, melanocytes, or melanoma cells for 24 h followed by MTS assay analysis. Untreated cells (−) served as controls for comparison. *Columns,* mean; *bars,* SE.

analysis of cellular protein lysates showed that siRNA designed specifically against ^{V600E}B-Raf reduced protein levels by ~50% in mutant UACC 903 (Fig. 2*A*) but not in wild-type B-Raf–expressing C8161.Cl9 cells (Fig. 2*B*). In contrast, siRNA designed to sequences present in both mutant and wild-type B-Raf decreased protein expression by ~75% in both cell lines (Fig. 2*A* and *B*). Similarly, siRNA that specifically targets Akt3 but not Akt1 or Akt2 has been reported, which can effectively decrease melanoma tumor development (6). Thus, siRNA designed to specifically inhibit mutant ^{V600E}B-Raf or Akt3 reduces the expression of mutant but not wild-type B-Raf protein and Akt3 but not Akt1 or Akt2, respectively (6).

siRNA targeting ^{V600E}B-Raf can be loaded into nanoliposomes, delivered into cells, and decrease expression of mutant protein. Having validated the specificity of siRNA targeting ^{V600E}B-Raf and Akt3, 1 μmol/L siRNA was loaded into nanoliposomes, and protein knockdown measured in 1205 Lu cells containing ^{V600E}B-Raf in three independent experiments by densitometric analysis and Western blotting (Fig. 2*C*). Examples of protein knockdown at 18 and 32 hours following a single treatment showed a 50% to 60% decrease of ^{V600E}B-Raf protein compared with cells treated with scrambled siRNA-nanoliposomal complex (Fig. 2*C*). Typically, protein knockdown ranged from 25% to 60%, indicating some variability, but knockdown was reproducibly observed. Duration of knockdown following a single siRNA treatment was measured by introducing siRNA into cells and using Western blotting to measure protein knockdown 2, 4, 6, and 8 days later. Western blots were densitometrically scanned and knockdown of B-Raf protein was compared with control cells nucleofected with siRNA targeting C-Raf. A consistent ~60% decrease in protein expression was observed through day 8 (Fig. 2*D*). Thus, siRNA specific to ^{V600E}B-Raf can be loaded into cationic nanoliposomes,

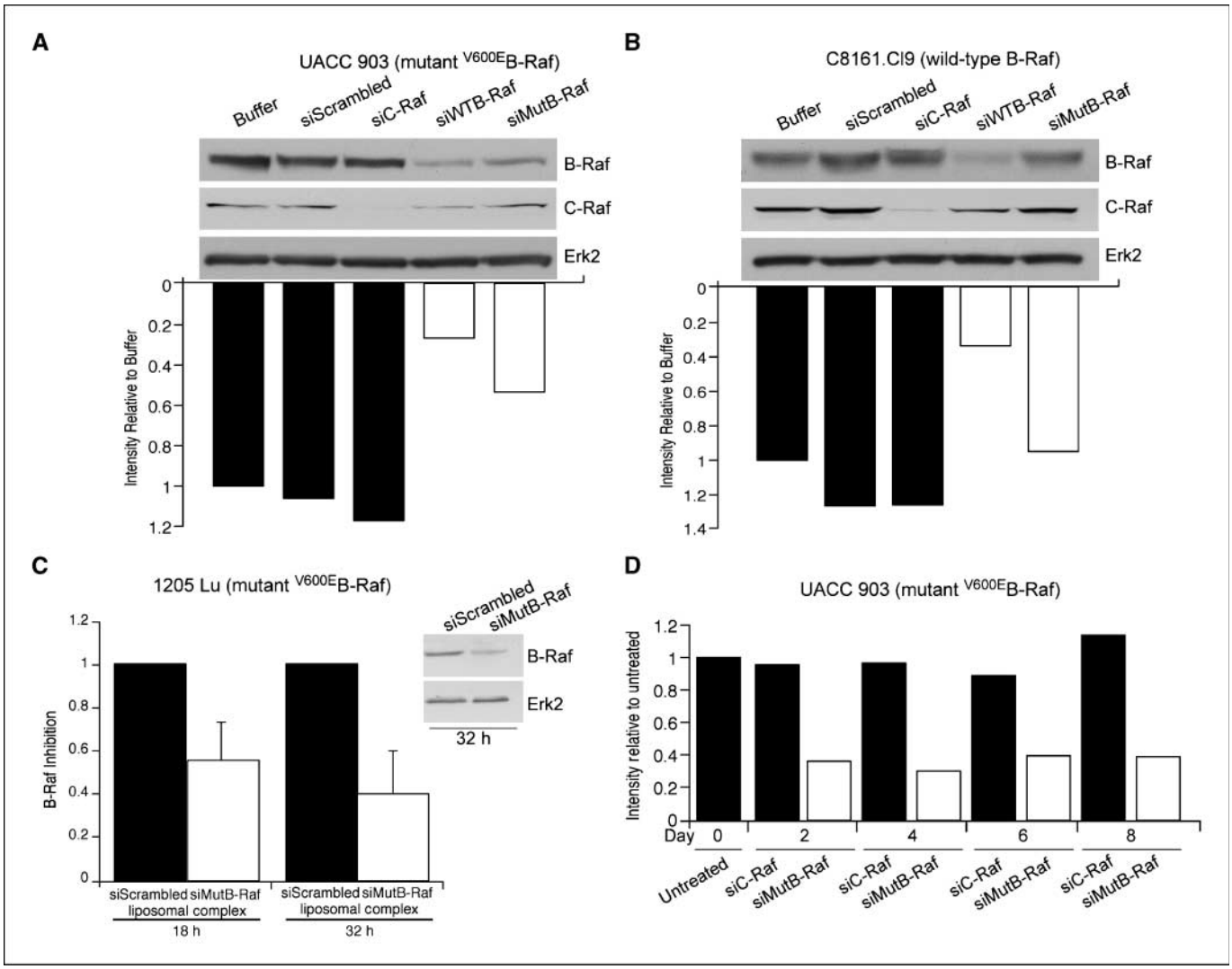

Figure 2. siMutB-Raf decreases protein expression of ^{V600E}B-Raf. *A* and *B,* siRNA can be designed to decrease ^{V600E}B-Raf expression but not normal protein expression. To verify specificity of siMutB-Raf for decreasing expression of mutant but not wild-type protein, melanoma cells containing mutant (UACC 903; *A*) or normal (C8161.Cl9; *B*) B-Raf protein were nucleofected with buffer, siScrambled, siC-Raf, siWTB-Raf, or siMutB-Raf siRNA; protein lysates were harvested 48 h later and analyzed by Western blot analysis for B-Raf and C-Raf knockdown. Erk2 served as a loading control. *C,* siMutB-Raf-nanoliposomal complex decreased the expression of ^{V600E}B-Raf protein in cells. 1205 Lu cells were exposed to siMutB-Raf or siScrambled-nanoliposomal complex; protein lysates were harvested at 18 and 32 h and analyzed by Western blot analysis. Erk2 served as a control for protein loading. *Columns,* mean; *bars,* SE. *D,* duration of ^{V600E}B-Raf protein knockdown following exposure to siRNA targeting mutant protein is beyond 8 d. Cells were nucleofected with C-Raf or ^{V600E}B-Raf siRNA and replated in culture dishes; protein was harvested 2, 4, 6, and 8 d later to measure duration of protein knockdown. Untreated cells or cells nucleofected with siRNA targeting C-Raf served as controls.

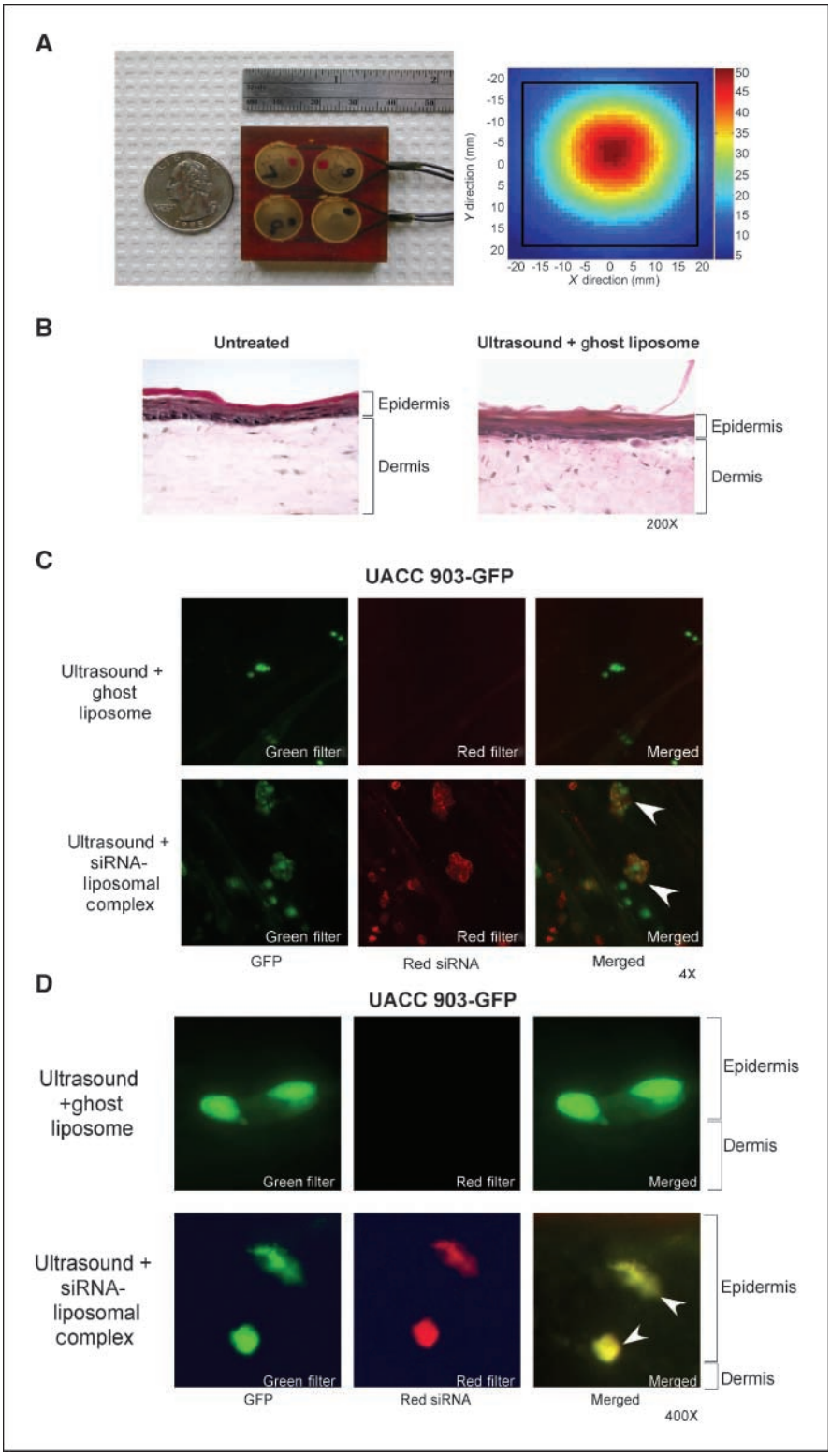

Figure 3. Ultrasound treatment permeabilizes skin, enabling melanocytic lesions to take up siRNA-nanoliposomal complexes. *A,* ultrasound assembly. A lightweight, low-profile ultrasound array was constructed using four-cymbal transducers, which were connected in parallel and encased in polymer. The temporal peak intensity was determined in a spatial plane 1 mm from the face of the transducer for exposure conditions. *B,* ultrasound treatment does not damage skin. Laboratory-generated skin was ultrasound treated followed by addition of ghost liposome, skin sectioned, and H&E stained. No changes in cellular structure or skin morphology were observed compared with untreated control skin (magnification, ×200). *C* and *D,* following ultrasound treatment of skin, siRNA-nanoliposomal complex is taken up by melanocytic lesions in the epidermis and at the epidermal-dermal junction. Following 20-min ultrasound treatment, fluorescent siRNA-nanoliposomal complex or ghost nanoliposomes were applied topically onto reconstructed skin. One hour later, skin was fixed and analyzed by fluorescence microscopy looking down at the skin (magnification, ×4; *C*) or by cross sections (magnification, ×400; *D*). Fluorescence (*red*) indicating the presence of siRNA-nanoliposomal complex was evident in melanocytic lesions in both epidermis and at epidermal-dermal junction (*arrows*).

delivered into melanoma cells, and decrease protein expression by 25% to 60% following a single treatment.

Ultrasound treatment of laboratory-generated skin containing melanocytic lesions enables delivery of siRNA-nanoliposomal complex into tumors. Skin forms a natural barrier that prevents uptake of agents including lipids and siRNA (19, 21). Therefore, skin was permeabilized before addition of siRNA-liposomal complex using a lightweight four-cymbal array ultrasound developed originally to deliver insulin through skin and into the blood stream (Fig. 3*A, left*; refs. 23–26). A representative exposimetry analysis showed a Gaussian-shaped peak field intensity with an overall spatial peak-temporal intensity of 50.6 ± 1.5 mW/cm^2

(Fig. 3*A, right*). Possible skin damage by ultrasound was evaluated on reconstructed skin treated with ultrasound for 20 minutes followed by addition of topically added ghost liposome for 1 hour followed by fixation. H&E-stained skin sections comparing untreated control to ultrasound- and ghost liposome–treated skin showed no detectable damage (Fig. 3*B*). Next, skin penetration by siRNA-nanoliposomal complex following ultrasound treatment was measured. Skin was ultrasound treated for 20 minutes followed by topical addition of liposome loaded with 1 μmol/L Alexa Fluor 546–tagged siRNA and, 1 hour later, fixed in 4% paraformaldehyde followed by analysis using fluorescence stereomicroscopy. Top-down views of the skin showed uptake of red Alexa Fluor 546–tagged siRNA in both keratinocytes and UACC 903-GFP melanoma cells (Fig. 3*C*). Cross sections of skin showed the presence of red Alexa Fluor 546–tagged siRNA in melanoma cells located in both epidermis and epidermal-dermal junction (Fig. 3*D*). Similar results were seen in skin reconstructs containing WM35-GFP (data not shown). Thus, permeabilizing skin using ultrasound before topical application of siRNA-nanoliposomal complex enabled delivery of siRNA to melanocytic lesions located within skin.

Following ultrasound treatment, nanoliposomal complex containing siRNA targeting ^{V600E}B-Raf inhibits melanocytic lesion development in skin reconstructs. The effectiveness of siRNA-nanoliposomal complex for inhibiting early melanocytic skin lesions or cutaneous metastasis development was examined by treating skin containing GFP tumors on alternate days with ultrasound for 20 minutes followed by addition of nanoliposomes containing siRNA to ^{V600E}B-Raf or ghost liposome (Fig. 4*A*). On day 21, stereo fluorescence microscopy was used to quantify average area occupied by GFP fluorescent skin lesions, which was compared with ultrasound + ghost liposome–treated skin. A statistically significant 50% to 65% reduction in area occupied was observed for WM35-GFP (Fig. 4*B*) and UACC 903-GFP (Fig. 4*C*) tumor nodules ($P < 0.05$, one-way ANOVA). The WM35 cell line represents early noninvasive melanocytic lesions, whereas UACC 903 cells represent invasive melanocytic lesions in the reconstructed skin model. Thus, siRNA-mediated inhibition of ^{V600E}B-Raf decreased the proliferative capacity of tumor cells, reducing skin nodule development.

Mechanistically, siRNA targeting ^{V600E}B-Raf decreases the proliferative potential of melanoma cells by inhibiting MAP kinase signaling in laboratory-generated skin. To establish the mechanistic basis by which siRNA targeting ^{V600E}B-Raf inhibited melanoma development, siRNA was introduced into GFP-tagged WM35 or UACC 903 cells, which were seeded into the epidermis of reconstructed skin. Ten days later, skin was fixed and fluorescence microscopy was used to quantify the average area occupied by

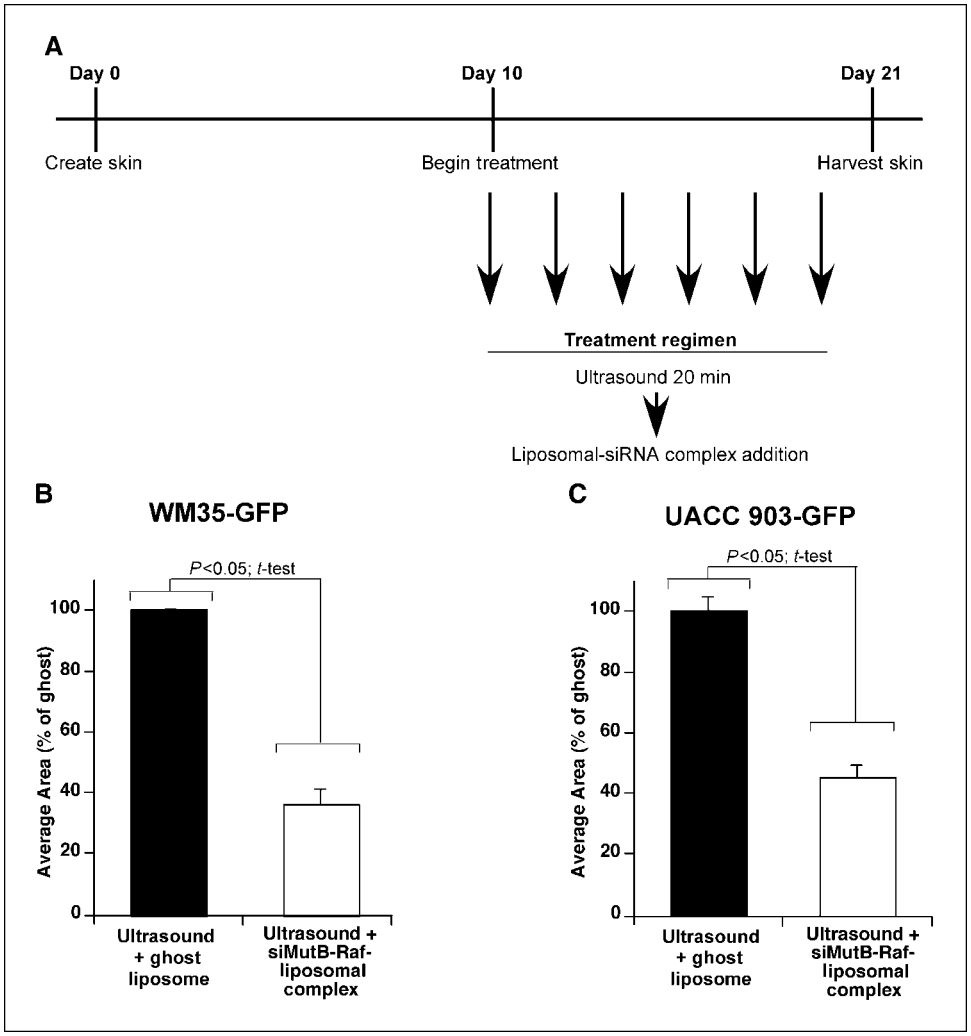

Figure 4. Ultrasound treatment followed by topical application of siMutB-Raf-nanoliposomal complex inhibits melanocytic lesion development in reconstructed skin. *A,* schematic showing treatment regimen. Beginning on day 10 and on alternate days thereafter up to day 20, reconstructed skin was treated with ultrasound for 20 min followed by topical administration of siMutB-Raf-nanoliposomal complex (100 pmol) or ghost nanoliposomes. *B* and *C,* ultrasound followed by addition of siMutB-Raf-nanoliposomal complex decreases melanocytic lesion development in skin. Reconstructed skin containing UACC 903-GFP or WM35-GFP cells was treated with ultrasound for 20 min followed by topical administration of siMutB-Raf-nanoliposomal complex on alternate days from days 10 to 20. Skin was harvested on day 21, and the average area occupied by GFP-tagged tumors was calculated for each group. Ultrasound treatments followed by exposure to ghost nanoliposomes served as a control. *Columns,* mean; *bars,* SE.

GFP-expressing tumor nodules. Compared with cells nucleofected with buffer, scrambled siRNA, or C-Raf siRNA, a 3- to 7-fold reduction in nodule development was observed by cells exposed to siRNA targeting ^{V600E}B-Raf (Fig. 5*A* and *B*; $P < 0.05$, one-way ANOVA). Knockdown of ^{V600E}B-Raf protein expression was confirmed by Western blotting of protein lysates collected following creation of reconstructed skin (Fig. 5*A* and *C*).

The mechanism leading to decreased cutaneous tumor development was established by calculating *in vitro* doubling times as well as comparing differences in proliferation and measuring the effect on MAP kinase signaling. siRNA-mediated inhibition of ^{V600E}B-Raf decreased mutant protein expression, causing corresponding decreases in phosphorylated MAP kinase/Erk kinase (pMek) and pErk as well as decreased cyclin D1 expression, indicating reduction in the proliferative signaling pathways of these cells (Fig. 5*A* and *C*). The doubling time of cultured cells containing siRNA targeting ^{V600E}B-Raf was found to be ~1.3-fold higher than that of control cells treated with buffer or scrambled siRNA (Fig. 5*D, left*). Furthermore, a 4- to 5-fold decrease in proliferating cells was observed in tumor cells treated with siRNA targeting ^{V600E}B-Raf compared with control cells treated with C-Raf siRNA (Fig. 5*D, right*). This growth-inhibitory mechanism is consistent with prior reports (8, 30). Thus, siRNA in nanoliposomes can decrease the expression of ^{V600E}B-Raf protein, reducing MAP kinase signaling and the proliferative potential of melanoma cells.

Following ultrasound treatment, siRNA-nanoliposomal complex targeting ^{V600E}B-Raf and Akt3 cooperatively decreased melanocytic lesion development in animal skin. The effect of ultrasound followed by topical application of nanoliposomal-siRNA complex on melanoma development in animal skin was examined next. UACC 903-GFP cells (1×10^6) were s.c. injected into the right flank of nude mice and, under anesthesia, treated on alternate days at the tumor site with ultrasound for 15 minutes followed by topical application of siRNA-nanoliposomal complex (Fig. 6*A*). Along with measurement of tumor size (Fig. 6*B*), mice were weighed (Fig. 6*B, inset*) on alternate days. The effects of liposomes containing siRNA targeting ^{V600E}B-Raf or Akt3 alone or ^{V600E}B-Raf and Akt3 together on tumor development were compared. Ghost liposomes were added to single treatments to compensate for differences in the amount of liposomal vehicle. A statistically significant ~30% reduction in tumor size was observed from day 15 in mice treated with complex containing siRNA targeting ^{V600E}B-Raf compared with animals exposed to complex containing scrambled siRNA (Fig. 6*B*; $P < 0.05$, two-way ANOVA). In contrast, no statistically significant difference was observed in cutaneous melanoma development following treatment with liposomes containing siRNA targeting Akt3 although treated tumors were 10% to 15% smaller than controls treated with liposomes containing scrambled siRNA (Fig. 6*B*; $P > 0.05$, two-way ANOVA). Significantly, the combination treatment showed cooperatively acting tumor inhibition from day 11 when compared with siScrambled-liposomal complex (Fig. 6*B*; $P < 0.05$, two-way ANOVA).

Weights were monitored on alternate days to ascertain weight-related toxicity (Fig. 6*B, inset*). No differences were seen in weights, indicating a lack of toxicity ($P > 0.05$, two-way ANOVA). The lack of systemic toxicity was confirmed by analyzing blood for ALT, AST, alkaline phosphatase, and glucose levels (data not shown), which showed no significant differences between animal groups ($P > 0.05$, *t* test). Additionally, no changes in liver morphology were detected in H&E-stained sections (data not shown).

Targeting ^{V600E}B-Raf and Akt3 leads to additively cooperative inhibition. Because liposomal-mediated targeting of Akt3 and ^{V600E}B-Raf suggested cooperatively acting tumor inhibition, the mechanistic basis for inhibition was determined. siRNA targeting Akt3 and/or ^{V600E}B-Raf was nucleofected into UACC 903 cells and the effect on *in vitro* anchorage-independent growth was examined. For these studies and subsequent Chou-Talalay analysis for measuring the mechanistic basis underlying inhibition, Akt3 siRNA was maintained at 200 pmol and B-Raf siRNA was titrated at doses of 3, 6, and 12 pmol. Simultaneous siRNA-mediated inhibition of Akt3 and B-Raf significantly decreased the growth of cells compared with either Akt3 or B-Raf targeting alone (Fig. 6*C*, *lanes 3* and *4* versus *lane 7, lanes 3* and *5* versus *lane 8*, and *lanes 3* and *6* versus *lane 9; P* < 0.05, one-way ANOVA; ref. 38).

To establish whether growth inhibition would be additive or synergistic following simultaneous inhibition of Akt3 and ^{V600E}B-Raf, the Chou-Talalay method was used for determining the combination index using Calcusyn software (35). Using this approach, combination index values <0.9 are synergistic, >1.1 is antagonistic, and values 0.9 to 1.1 are additive (Fig. 6*D*). The estimated combination index values were 0.94, 0.97, and 1.10, for 3, 6, and 12 pmol of B-Raf siRNA plus 200 pmol of Akt3 siRNA, suggesting additive cooperation (Fig. 6*D*). Thus, targeting ^{V600E}B-Raf and Akt3 in culture or in animals should lead to cooperatively additive inhibition. However, tumor inhibition following liposome-mediated delivery of siRNA targeting ^{V600E}B-Raf and Akt3 in Fig. 6*B* seems to be more than additive, suggesting that it may tend toward being synergistic.

Discussion

Novel therapeutic regimens need to be developed for treating early or cutaneous metastatic melanoma because, aside from surgical excision, few treatment options are available (39). Current systemic therapeutics cause toxicities and have off-target effects (19). Topical or localized treatments with agents could permit use of high local concentrations with minimal toxicity and be useful for treating cutaneous lesions not amenable to surgical removal (19, 40). A case in point is the use of interlesional injections of interleukin 2 (IL-2) and electroporation for improved topical delivery of bleomycin for melanoma treatment (40, 41). Effective topical agents could provide additional, currently unavailable, treatment options for patients with early or invasive cutaneous melanoma.

The era of personalized, targeted cancer treatment is near, but specific proteins playing key roles in particular cancer types need identification and the demonstration that simultaneous targeting inhibits tumor development in a synergistic manner. This study shows that ^{V600E}B-Raf and Akt3 are two such targets in melanoma, the inhibition of which led to cooperative tumor inhibition. Furthermore, a novel approach has been developed for delivering therapeutic siRNA into early or invasive cutaneous melanocytic lesions targeting these important proteins. Ultrasound treatment of skin followed by topical application of nanoliposomes containing siRNA targeting ^{V600E}B-Raf and Akt3 reduced the expression of these proteins, significantly decreasing melanoma development in a cooperatively additive manner.

Simultaneous inhibition of the MAP and phosphatidylinositol 3-kinase pathways has previously been reported to enhance the inhibitory effect on both signaling cascades leading to increased tumor cell apoptosis, which supports the feasibility of this

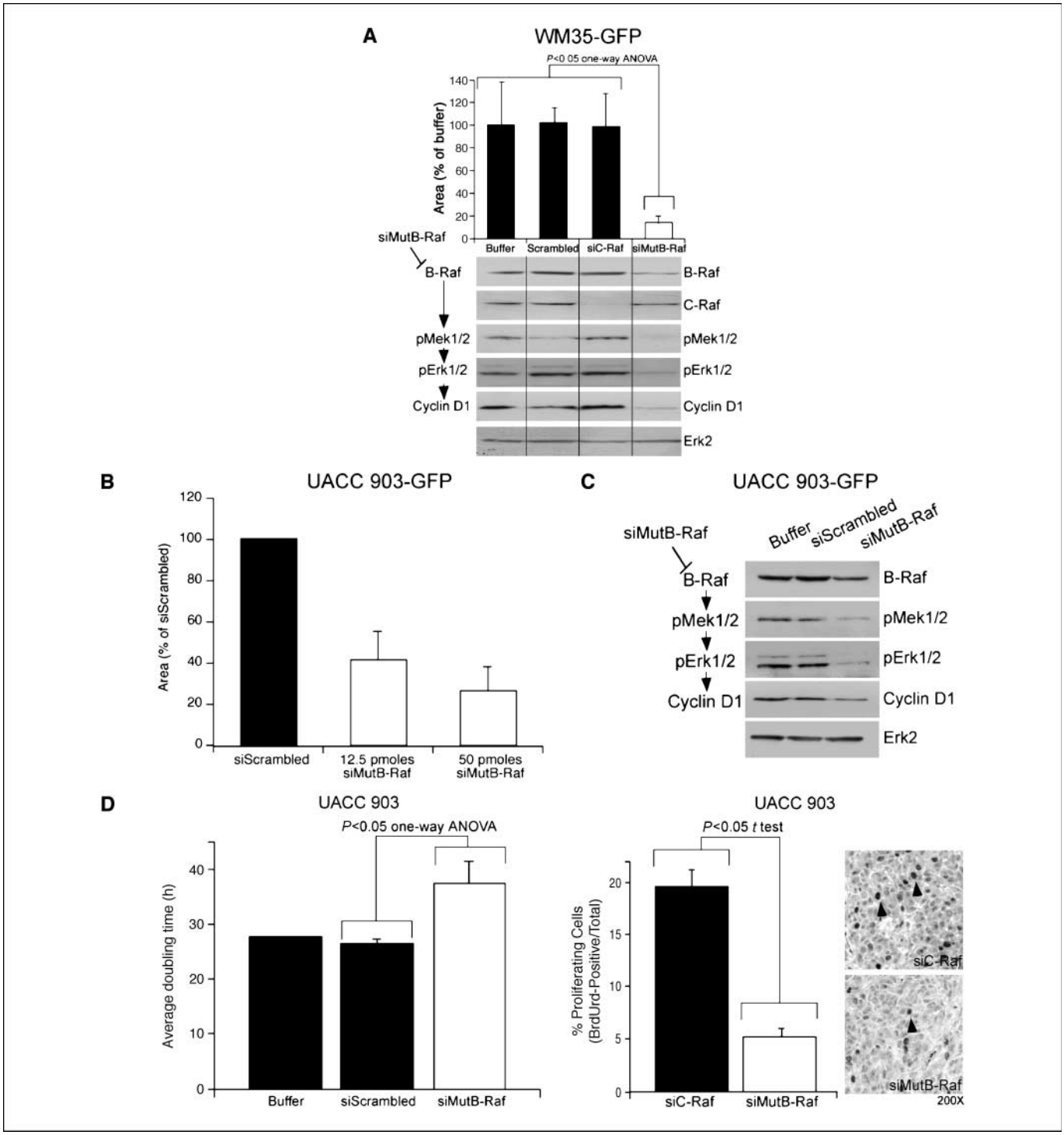

Figure 5. siMutB-Raf inhibits melanocytic lesion growth in reconstructed skin. *A,* targeting melanocytic lesions using siRNA against ^{V600E}B-Raf decreases melanocytic lesion development in laboratory-generated skin. The effectiveness of siRNA targeting ^{V600E}B-Raf for decreasing cutaneous tumor development was established by nucleofecting GFP-tagged WM35 cells with buffer, scrambled siRNA, or siRNA targeting C-Raf or ^{V600E}B-Raf (100 pmol). Cells were then seeded into laboratory-generated skin at time of creation and, 10 d later, average area occupied by green melanocytic lesions was quantified. *Top,* a statistically significant reduction in green fluorescent lesions was observed following siMutB-Raf treatment ($P < 0.05$, one-way ANOVA). *Columns,* mean; *bars,* SE. *Bottom,* protein lysates harvested from cells were analyzed by Western blot for B-Raf, C-Raf, pMek1/2, pErk1/2, and cyclin D1 protein expression. Erk2 served as a control for protein loading. *B,* siRNA-mediated inhibition of ^{V600E}B-Raf protein expression in GFP-tagged UACC 903 cells decreases lesion formation in skin reconstructs. UACC 903-GFP cells were nucleofected with siScrambled or siB-Raf (12.5 or 50 pmol) and cells were seeded into laboratory-generated skin at time of creation. Reconstructed skin was analyzed by fluorescence microscopy 10 d later and area occupied by developing GFP lesions was quantified. *Columns,* mean; *bars,* SE. *C,* inhibition of ^{V600E}B-Raf decreased MAP kinase signaling in UACC 903-GFP cells. UACC 903-GFP cells were nucleofected with buffer, siScrambled, or siB-Raf (50 pmol) and harvested at 48 h for Western blot analysis. Westerns were probed with B-Raf, pMek1/2, pErk1/2, and cyclin D1 to show decreased MAP kinase pathway signaling. Erk2 served as a loading control. *D,* mechanistically, siRNA-mediated targeting of ^{V600E}B-Raf protein decreased the proliferative capacity of cells. Cultured UACC 903 melanoma cells treated with siMutB-Raf had an increased doubling time, indicating that cells were proliferating at a slower rate (*left*). Quantifying proliferating cells showed a 2- to 3-fold decrease following siMutB-Raf treatment of tumor cells compared with size- and time-matched tumor controls treated with siRNA to C-Raf (*middle* and *right*). *Columns,* mean; *bars,* SE.

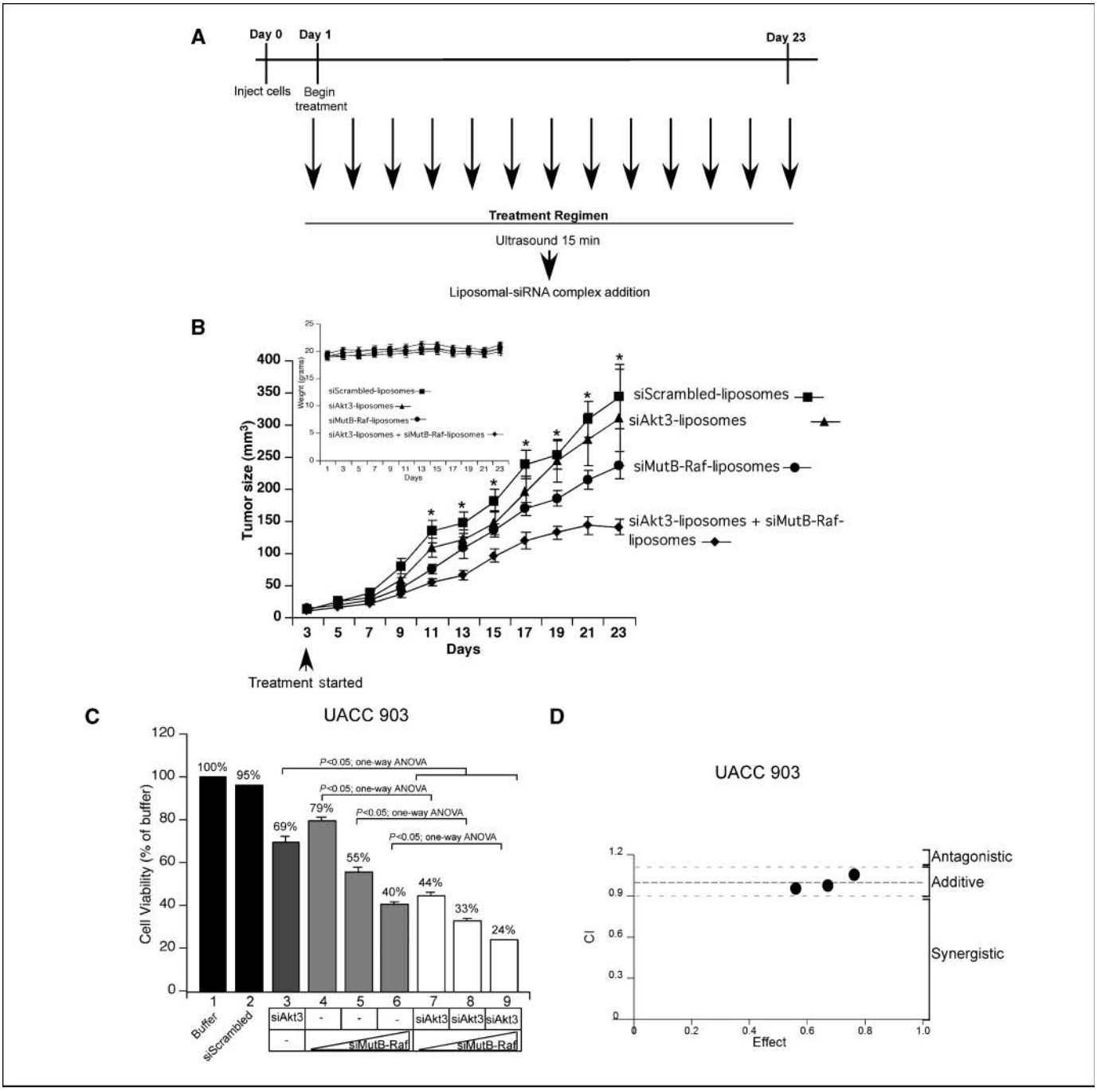

Figure 6. Ultrasound treatment followed by topical application of siMutB-Raf-nanoliposomal complex alone or in combination with siAkt3-nanoliposomal complex inhibits melanocytic lesion development in animal skin. *A,* schematic showing treatment regimen. Ultrasound treatment followed by topical application of siMutB-Raf-nanoliposomal complexes that was started the day after injection of melanoma cells and continued on alternate days up to day 23. During the procedure, anesthetized mice were treated with ultrasound at the injection site for 15 min followed by topical application of siMutB-Raf-nanoliposomal complex. *B,* ultrasound treatment followed by topical application of siAkt3-liposomal complex + siMutB-Raf-liposomal complex decreased melanoma development in animal skin. UACC 903-GFP cells (1×10^6) were injected s.c. into nude mice and, after 24 h, tumors forming at injection sites were treated on alternate days with ultrasound for 15 min followed by topical administration of siMutB-Raf-liposomal complex, siAkt3-liposomal complex, or siAkt3-liposomal complex + siMutB-Raf liposomal complex. Tumors were measured on alternate days beginning on day 3. Control mice were ultrasound treated followed by addition of siScrambled-liposomal complex. Ghost liposomes were added to single treatments so that mice were treated with equivalent amounts of liposomal vehicle. Statistically significant differences between control and siMutB-Raf-liposomal complex + siAkt3-liposomal complex–treated tumors were observed beginning on day 11 ($P < 0.05$, two-way ANOVA). *Columns,* mean; *bars,* SE. Ultrasound treatment followed by topical application of siAkt3-liposomal complex + siMutB-Raf-liposomal complex does not cause a significant change in animal body weight. Animal weights were measured on alternate days beginning on day 1 to determine whether any weight-related toxicity occurred. No significant weight loss was observed between control and experimental groups ($P > 0.05$, two-way ANOVA; *B, inset*). *Points,* mean; *bars,* SE. *C,* siMutB-Raf and siAkt3 cooperate to reduce anchorage-independent growth in cell culture. UACC 903 cells were nucleofected with siAkt3 (200 pmol) and siMutB-Raf (1.5, 3, 6, or 12 pmol) in combination and compared with single siRNAs to siAkt3 (200 pmol), siMutB-Raf (1.5, 3, 6, or 12 pmol), siScrambled, or buffer only for the ability to inhibit anchorage-independent growth. *D,* siAkt3 and siMutB-Raf act additively to inhibit cell viability. Calculation of the combination index (*CI*) for the combination of siAkt3 and siMutB-Raf showed additive inhibition of cell viability with combination index values between 0.94 and 1.10.

approach (42–44). Furthermore, siRNA-mediated inhibition of ^{V600E}B-Raf and Akt3 in aggressive melanoma cells has been shown to cooperatively inhibit tumor development through enhanced effects on the signaling cascades, specifically leading to decreased cyclin D1 expression as well as increased p27 and cleaved caspase-3 levels (9). These results are not surprising considering discoveries linking the two pathways in early melanoma development (9). Approximately 90% of nevi express ^{V600E}B-Raf, but very few ever develop into melanoma due to the inhibitory effects associated with high MAP kinase pathway activity caused by the mutant protein. Akt3 has been shown to overcome this block by phosphorylating ^{V600E}B-Raf in these melanocytes to lower the activity of mutant protein and downstream MAP kinase pathway signaling to levels promoting, rather than inhibiting, melanoma development (9). Phosphorylation of ^{V600E}B-Raf enabled melanocytes to overcome the growth-inhibitory effects associated with high pathway activity and to develop melanoma cell–like characteristics (9). Thus, this discovery shows that siRNA can be used as a therapeutic specifically targeting multiple aberrantly expressed or mutant cancer-causing genes without inhibiting the activity of normal proteins to more effectively treat melanoma.

Systemic administration of free unmodified siRNA by i.v. injection is not clinically feasible because it is rapidly degraded by serum factors, preventing clinically useful concentrations from being reached (45). Development of novel vehicles for loading, protecting, and delivering siRNA to distant sites around the body is one strategy (16–18, 46, 47). This study shows that cationic nanoliposomes can load, protect, and deliver therapeutic siRNA into melanoma cells. Nanoliposomes are taken up by all cell types but only affects those containing ^{V600E}B-Raf or overexpressing Akt3. The specificity of siRNA for its target reduces toxicity and potential side effects. Furthermore, use of pegylated lipids and small average nanoliposomes with a diameter of $\sim$50 nm decreases immunologic or inflammatory responses, enabling the particles to bypass the reticulo-endothelial system (48, 49).

Ultrasound was used to permeabilize skin, enabling delivery of siRNA-liposomal complex throughout the epidermal and dermal layers because it had been reported to be effective for delivering various macromolecules into and throughout skin (19, 21–26). A lightweight transducer with shown capabilities of delivering insulin or antisense oligonucleotides into or through skin was used, showing that low-frequency ultrasound can permeabilize skin, enabling delivery of nanoliposomal-siRNA into melanoma cells residing at the dermal-epidermal junction to inhibit protein expression and melanoma development.

Mechanistically, a therapeutic nanoliposomal-siRNA complex targeting ^{V600E}B-Raf and Akt3 can effectively decrease the expression of both proteins and downstream signaling cascades to inhibit the development or spread of cutaneous melanoma (8, 10, 30). Thus, a nanoliposomal-siRNA complex targeting these proteins could be used as a nonsurgical approach to decrease the number of benign moles or inhibit early cutaneous melanocytic lesion development (2–5, 9). The latter would have the consequence of decreasing the spread at the earliest stages, thereby prolonging survival by preventing metastases. Ultrasound in conjunction with a therapeutic topical nanoliposomal-siRNA complex targeting ^{V600E}B-Raf and Akt3 could also provide a treatment option for patients whose disease is not amenable to surgical removal or limb perfusion when widespread cutaneous lesions are present on the trunk. No therapeutic agents for treating these patients are available. Furthermore, advanced-stage melanoma patients could benefit by administering these agents at the time of sentinel lymph node biopsy or surgery to target cells that may not have been removed during the procedure (50). Finally, this approach could be combined with more traditional therapeutic agents to improve clinical efficacy through synergistically acting mechanisms.

In conclusion, topical delivery of cationic nanoliposomes loaded with siRNA targeting ^{V600E}B-Raf and Akt3 in combination with low-frequency ultrasound has potential to decrease early melanocytic lesion development in skin or prevent the spread of cutaneous melanoma metastases.

Disclosure of Potential Conflicts of Interest

M. Kester: ownership interest, Keystone Nano. The other authors disclosed no potential conflicts of interest.

Acknowledgments

Received 12/11/2007; revised 6/6/2008; accepted 7/2/2008.

Grant support: NIH/National Cancer Institute grant 1-RO3-CA128033-01, American Cancer Society grant RSG-04-053-01-GMC, The Foreman Foundation for Melanoma Research, State of Pennsylvania Non-formulary Tobacco Settlement Funds, and Department of Defense Technologies for Metabolic Monitoring grant W81XWH-05-1-0617.

The costs of publication of this article were defrayed in part by the payment of page charges. This article must therefore be hereby marked *advertisement* in accordance with 18 U.S.C. Section 1734 solely to indicate this fact.

We thank James Kaiser, Julie Anderson, Nishit Trivedi, Mitchel Cheung, and SubbaRao V. Madhunpantula for technical assistance, and Shantu Amin for critical reading of the manuscript.

References

1. Satyamoorthy K, Herlyn M. Cellular and molecular biology of human melanoma. Cancer Biol Ther 2002;1:14–7.
2. Brose MS, Volpe P, Feldman M, et al. BRAF and RAS mutations in human lung cancer and melanoma. Cancer Res 2002;62:6997–7000.
3. Davies H, Bignell GR, Cox C, et al. Mutations of the BRAF gene in human cancer. Nature 2002;417:949–54.
4. Yazdi AS, Palmedo G, Flaig MJ, et al. Mutations of the BRAF gene in benign and malignant melanocytic lesions. J Invest Dermatol 2003;121:1160–2.
5. Miller CJ, Cheung M, Sharma A, et al. Method of mutation analysis may contribute to discrepancies in reports of (V599E)BRAF mutation frequencies in melanocytic neoplasms. J Invest Dermatol 2004;123:990–2.
6. Stahl JM, Sharma A, Cheung M, et al. Deregulated Akt3 activity promotes development of malignant melanoma. Cancer Res 2004;64:7002–10.
7. Stahl JM, Cheung M, Sharma A, Trivedi NR, Shanmugam S, Robertson GP. Loss of PTEN promotes tumor development in malignant melanoma. Cancer Res 2003;63:2881–90.
8. Sharma A, Trivedi NR, Zimmerman MA, Tuveson DA, Smith CD, Robertson GP. Mutant V599EB-Raf regulates growth and vascular development of malignant melanoma tumors. Cancer Res 2005;65:2412–21.
9. Cheung M, Sharma A, Madhunapantula SV, Robertson GP. Akt3 and mutant (V600E) B-Raf cooperate to promote early melanoma development. Cancer Res 2008;68:3429–39.
10. Hingorani SR, Jacobetz MA, Robertson GP, Herlyn M, Tuveson DA. Suppression of BRAF(V599E) in human melanoma abrogates transformation. Cancer Res 2003;63:5198–202.
11. Brazas RM, Hagstrom JE. Delivery of small interfering RNA to mammalian cells in culture by using cationic lipid/polymer-based transfection reagents. Methods Enzymol 2005;392:112–24.
12. Gresch O, Engel FB, Nesic D, et al. New non-viral method for gene transfer into primary cells. Methods 2004;33:151–63.
13. Muratovska A, Eccles MR. Conjugate for efficient delivery of short interfering RNA (siRNA) into mammalian cells. FEBS Lett 2004;558:63–8.
14. Kim DH, Rossi JJ. Strategies for silencing human disease using RNA interference. Nat Rev Genet 2007;8:173–84.
15. Leung RK, Whittaker PA. RNA interference: from gene silencing to gene-specific therapeutics. Pharmacol Ther 2005;107:222–39.
16. Zhang C, Tang N, Liu X, Liang W, Xu W, Torchilin VP. siRNA-containing liposomes modified with polyarginine effectively silence the targeted gene. J Control Release 2006;112:229–39.

17. Halder J, Kamat AA, Landen CN, Jr., et al. Focal adhesion kinase targeting using *in vivo* short interfering RNA delivery in neutral liposomes for ovarian carcinoma therapy. Clin Cancer Res 2006;12:4916–24.
18. Pal A, Ahmad A, Khan S, et al. Systemic delivery of RafsiRNA using cationic cardiolipin liposomes silences Raf-1 expression and inhibits tumor growth in xenograft model of human prostate cancer. Int J Oncol 2005;26: 1087–91.
19. El Maghraby GM, Williams AC, Barry BW. Can drug-bearing liposomes penetrate intact skin? J Pharm Pharmacol 2006;58:415–29.
20. Lee SH, Jeong SK, Ahn SK. An update of the defensive barrier function of skin. Yonsei Med J 2006;47:293–306.
21. Ting WW, Vest CD, Sontheimer RD. Review of traditional and novel modalities that enhance the permeability of local therapeutics across the stratum corneum. Int J Dermatol 2004;43:538–47.
22. Lavon I, Kost J. Ultrasound and transdermal drug delivery. Drug Discov Today 2004;9:670–6.
23. Lee S, Newnham RE, Smith NB. Short ultrasound exposure times for noninvasive insulin delivery in rats using the lightweight cymbal array. IEEE Trans Ultrason Ferroelectr Freq Control 2004;51:176–80.
24. Park EJ, Werner J, Smith NB. Ultrasound mediated transdermal insulin delivery in pigs using a lightweight transducer. Pharm Res 2007;24:1396–401.
25. Smith NB, Lee S, Maione E, Roy RB, McElligott S, Shung KK. Ultrasound-mediated transdermal transport of insulin *in vitro* through human skin using novel transducer designs. Ultrasound Med Biol 2003;29:311–7.
26. Smith NB, Lee S, Shung KK. Ultrasound-mediated transdermal *in vivo* transport of insulin with low-profile cymbal arrays. Ultrasound Med Biol 2003;29:1205–10.
27. Satyamoorthy K, DeJesus E, Linnenbach AJ, et al. Melanoma cell lines from different stages of progression and their biological and molecular analyses. Melanoma Res 1997;7 Suppl 2:S35–42.
28. Stover T, Kester M. Liposomal delivery enhances short-chain ceramide-induced apoptosis of breast cancer cells. J Pharmacol Exp Ther 2003;307:468–75.
29. Stover TC, Sharma A, Robertson GP, Kester M. Systemic delivery of liposomal short-chain ceramide limits solid tumor growth in murine models of breast adenocarcinoma. Clin Cancer Res 2005;11:3465–74.
30. Sharma A, Tran MA, Liang S, et al. Targeting mitogen-activated protein kinase/extracellular signal-regulated kinase kinase in the mutant (V600E) B-Raf signaling cascade effectively inhibits melanoma lung metastases. Cancer Res 2006;66:8200–9.
31. Rasband WS. ImageJ. Bethesda (MD): U.S. National Institutes of Health; 1997-2007.
32. Meyers C. Organotypic (raft) epithelial tissue culture system for the differentiation-dependent replication of papillomavirus. Methods Cell Sci 1996;18:201–10.
33. Maione E, Shung KK, Meyer RJ, Jr., Hughes JW, Newnham RE, Smith NB. Transducer design for a portable ultrasound enhanced transdermal drug-delivery system. IEEE Trans Ultrason Ferroelectr Freq Control 2002;49:1430–6.
34. Newnham RE, Dogan A, inventors; Metal-electroactive ceramic composite transducer patent 5,729,077; 1998.
35. Chou TC, Talalay P. Quantitative analysis of dose-effect relationships: the combined effects of multiple drugs or enzyme inhibitors. Adv Enzyme Regul 1984;22: 27–55.
36. RNA interference—technical reference and application guide. Lafayette (CO): Dharmacon, Inc.; 2004.
37. Cory AH, Owen TC, Barltrop JA, Cory JG. Use of an aqueous soluble tetrazolium/formazan assay for cell growth assays in culture. Cancer Commun 1991;3:207–12.
38. Christensen C, Guldberg P. Growth factors rescue cutaneous melanoma cells from apoptosis induced by knockdown of mutated (V600E) B-RAF. Oncogene 2005; 24:6292–302.
39. Garbe C, Eigentler TK. Diagnosis and treatment of cutaneous melanoma: state of the art 2006. Melanoma Res 2007;17:117–27.
40. Radny P, Caroli UM, Bauer J, et al. Phase II trial of intralesional therapy with interleukin-2 in soft-tissue melanoma metastases. Br J Cancer 2003;89:1620–6.
41. Mir LM, Glass LF, Sersa G, et al. Effective treatment of cutaneous and subcutaneous malignant tumours by electrochemotherapy. Br J Cancer 1998;77:2336–42.
42. Bedogni B, O'Neill MS, Welford SM, et al. Topical treatment with inhibitors of the phosphatidylinositol 3′-kinase/Akt and Raf/mitogen-activated protein kinase kinase/extracellular signal-regulated kinase pathways reduces melanoma development in severe combined immunodeficient mice. Cancer Res 2004;64: 2552–60.
43. Bedogni B, Welford SM, Kwan AC, Ranger-Moore J, Saboda K, Powell MB. Inhibition of phosphatidylinositol-3-kinase and mitogen-activated protein kinase kinase 1/2 prevents melanoma development and promotes melanoma regression in the transgenic TPRas mouse model. Mol Cancer Ther 2006;5: 3071–7.
44. Smalley KS, Haass NK, Brafford PA, Lioni M, Flaherty KT, Herlyn M. Multiple signaling pathways must be targeted to overcome drug resistance in cell lines derived from melanoma metastases. Mol Cancer Ther 2006;5:1136–44.
45. Behlke MA. Progress towards *in vivo* use of siRNAs. Mol Ther 2006;13:644–70.
46. Sorensen DR, Leirdal M, Sioud M. Gene silencing by systemic delivery of synthetic siRNAs in adult mice. J Mol Biol 2003;327:761–6.
47. Derfus AM, Chen AA, Min DH, Ruoslahti E, Bhatia SN. Targeted quantum dot conjugates for siRNA delivery. Bioconjug Chem 2007;18:1391–6.
48. Gabizon A, Catane R, Uziely B, et al. Prolonged circulation time and enhanced accumulation in malignant exudates of doxorubicin encapsulated in polyethylene-glycol coated liposomes. Cancer Res 1994; 54:987–92.
49. Treat J, Damjanov N, Huang C, Zrada S, Rahman A. Liposomal-encapsulated chemotherapy: preliminary results of a phase I study of a novel liposomal paclitaxel. Oncology (Huntingt) 2001;15:44–8.
50. Balch CM. Cutaneous melanoma. 3rd ed. St. Louis (MO): Quality Medical Pub.; 1998.

Targeting ^{V600E}B-Raf and Akt3 Using Nanoliposomal-Small Interfering RNA Inhibits Cutaneous Melanocytic Lesion Development

Melissa A. Tran, Raghavendra Gowda, Arati Sharma, et al.

Cancer Res 2008;68:7638-7649.